

**Evaporative Mass Loss Measurement as a Quality Control Tool for Quality Assurance in the
Manufacture of Inks Suitable for High Speed (≥ 60 m/min) Printing**

Haydn J. Ward,^{*1,2,3} Tobias A. Armstrong-Telfer,^{2,3} Stephen M. Kelly,^{4,5}
Nathan S. Lawrence,^{3,5} Jay D. Wadhawan^{*3,4,5}

¹*Department of Physics & Mathematics, The University of Hull,
Cottingham Road, Kingston-upon-Hull HU6 7RX, United Kingdom.*

²*BemroseBooth Paragon, Ltd., Stockholm Road,
Kingston-upon-Hull HU7 0XY, United Kingdom.*

³*Department of Chemical Engineering, The University of Hull,
Cottingham Road, Kingston-upon-Hull HU6 7RX, United Kingdom.*

⁴*Department of Chemistry, The University of Hull,
Cottingham Road, Kingston-upon-Hull HU6 7RX, United Kingdom.*

⁵*Aura Innovation Centre, Bridgehead Business Park,
Meadow Road, Hessle HU13 0GD, United Kingdom.*

To be submitted to *J. Electroanal. Chem.*:

Special Issue in Honour of Professor Richard G. Compton

*Corresponding authors.

E.mail: haydn.ward@paragon-id.com (HJW); j.wadhawan@hull.ac.uk (JDW)

Abstract

In any manufacturing environment, it is always important to be able to embrace a culture of traceability of any non-conformed product. For the case of ink manufacture, operator confusion, leading to the mixing-up of solvents, or connecting the incorrect solvent drum to solvent lines, can lead to disastrous consequences that are not trivial for a quality control/quality assurance team to unravel. Accordingly, simple methods for assessing whether the correct solvents were added in the correct ratios to products empower this QA/QC requirement. In this paper, we examine the use of a trivial measurement of evaporative mass loss as a protocol for validating the conformance of manufactured ink to specification. Inspired by the transport-limit that occurs at ultramicroelectrodes in electrochemistry, we develop theory to analyse evaporation rate measurements, and illustrate how vaporisation at the liquid | gas interface is dominated by a diffusion anisotropy, owing to natural convection for organic solvents, manufactured resins and commercialised inks that have been used, *inter alia*, for the underground transport tickets in the cities of London and Paris. We further demonstrate that the use of incorrect solvents is readily seen through evaporation rate transients, thereby enabling this measurement for human factor mitigation during the ink manufacture process.

Key words: Evaporation, natural convection, quality control and quality assurance, mass transport, mass transit tickets, anisotropic diffusion, printing inks, analytical chemistry, chemical analysis.

1. Introduction

Since 2014, our team has developed and commercialised approximately 20 ink formulations suitable for high speed ($\geq 60 \text{ m min}^{-1}$) printing using gravity coaters, rotogravure or even flexographic presses. Such printing techniques, which are considerably faster than the silk screen printing often employed in electrochemistry [1,2] (which runs at speeds of typically *ca.* 5 m min^{-1}), are suitable for the low cost, high volume print runs needed for the fast-moving consumer goods markets. Indeed, our inks have been predominantly sold to provide security applications for the mass transit market, and involve either magnetic and/or conductive features. Together with a bespoke ATEX Zone 1 rated manufacturing facility and QA/QC laboratory that we have designed, developed and realised in Hull through a Knowledge Transfer Partnership with BemroseBooth Paragon, approximately 200 tonnes of ink are formulated each year for use in printed goods in four continents; our markets have included the UK railway network (at *ca.* one billion tickets per year), Irish Rail, the metro railway systems of London, Paris (at *ca.* 600 million tickets per year), New York, Cairo, Caracas and Tyne and Wear, the motorway toll tickets in France and the bus lines in Poland and Phoenix (USA), and has led to our team being recognised through receiving a number of awards for business impact.[†]

Our ink manufacturing process is illustrated schematically in the flow diagram given in Figure 1. It is a batch process and involves the wet milling of ferrimagnetic and/or conductive pigments with surfactants, defoamers and particulate fillers dissolved, or suspended, in a number of organic solvents (*q.v.* Table 1 [3-13]) for several hours, followed by a “let-down” phase in which a resin, comprising a binder dissolved in an organic solvent, is blended into the suspension [14-16], so as to afford a thick slurry, that conforms to particular specifications (viscosity, solid weight content, rheology, *etc.*), based on the printing/coating application and customer specification (coercivity, squareness, surface resistivity, *etc.*), when transferred and dried onto a particular substrate. The exact compositions of the inks are proprietary information, but in general are dispersions of the pigments with wetting agents, secondary pigments, resins, lubricants, surfactants and other additives to reduce syneresis – the separation of liquid solvent from the dispersion [14]. Our manufacturing protocols and procedures have been designed in compliance with ISO 9001 and ISO 14001 standards pertaining to quality and waste management, so that the finished goods meet customer expectations, and the manufacturing process conforms to local environmental regulations.

Although the processes that we have developed are semi-automated, operators are employed during the manufacture, to undertake the various stages of material weighing and transfer, testing of the goods to ascertain stage-ends, and for the dispensing of the product (*q.v.* Figure 1). Accordingly, there is an opportunity for human error (such as operator confusion in mixing-up solvents, or in incorrectly connecting solvent drums to specific solvent lines) within the manufacturing system that, in the spirit of embracing a culture of cradle-to-grave product traceability, necessitates quality control (QC) experiments for the quality assurance (QA) of the manufactured product. Indeed, mixing up solvents

[†]A recent award, for example, was for Business Impact at the 2019 KTP Best of the Best Awards, *q.v.* <https://www.gov.uk/government/news/ktp-best-of-the-best-2019-winners-announced> (accessed on January 15, 2020).

for some of our formulations can lead to disastrous consequences in terms of solvent “run-through” of the printed boards, the “picking” of printed goods during windings, the “pin holing” and “feathering” of the print, and in the creation of poorly dispersed ink products (“clumping”). Such errors can be expensive and may lead to production losses on press time, or, worse, production downtime due to press failure. However, they can be overcome through monitoring the solvents used, during, or post-manufacture, using analytical techniques such as NMR, as we have done in the past [17].

In this paper, we develop a more pragmatic, “rough and rugged”, inexpensive, human factor quality control tool, that has been used to reassure both manufacturing operators and QA/QC technical staff that the correct solvents were used in the correct ratios during the manufacture of our products. This tool exploits the measurement of solvent evaporation rates, and uses simple experimental protocols and equipment, to generate data, which can be compared with standard measurements. This tool, exploiting mass transfer across a liquid | gas interface has been inspired by the transport regimes that occur at the solid | liquid, and liquid | liquid interfaces familiar to electrochemists [18-20].

We first consider evaporative mass transfer from a circular liquid disc, limited by gas-phase transport, to provide insight into experimental evaporation transients from neat solvents used in our manufacturing processes, followed by “real world” samples such as manufactured resins used in the let-down phase which we have used for inks for London Underground and Paris Métropolitain tickets, and final ink products – we use two different inks that are printed on British Rail tickets and on the tickets used for the bus services in Poland.

2. Experimental

2.1 Materials

All chemical materials employed in this work (solvents, resins and inks) were supplied by BemroseBooth Paragon, Ltd. through two Knowledge Transfer Partnerships (Programme Numbers 9576 and 10844). These materials were used as received, without any further purification. These solvents were *iso*-propyl acetate (IPAC), methyl ethyl ketone (MEK), tetrahydrofuran (THF) and toluene. The resins used, AR01 and HR01, were prepared as part of our manufacturing process and are, respectively, used in the formulations of magnetic inks used for printing the information stripe on the tickets of the Paris Métropolitain and the London Underground. The low coercivity magnetic ink formulation used, HL0301, is currently used to produce the magnetic stripe, *via* gravity-fed coating, on British Rail tickets; the high coercivity magnetic ink formulation employed in this work, HH0501, was developed for the tickets used on Polish buses.

2.2 Methods

This work employed a modified Stefan-Winklemann tube [21,22], fabricated from PTFE. It comprises a “pot” that is a 5.4 cm diameter cylinder, of length 5.4 cm, and was machined with a 2.0 cm diameter ($2r_0$) hole cored centrally, to a depth of around 4 cm. The size of this core was made to be sufficiently large for the liquid phase to be tested (viscous inks and resins, or organic solvents) to be poured easily into the cored volume, and to be subsequently removed through solvent washing after the experiment. The liquid to be tested was stirred rapidly (to overcome any syneresis) and was then poured into the pot, and the surface scraped with a sheet of polyethylene terephthalate, such that the liquid surface was levelled to the insulation. Ignoring meniscus effects, this allowed for the liquid level to be flush with the top part of the insulation. The width of the insulation (1.7 cm) around the circumference of the liquid was chosen to be at least twice the steady-state diffusion layer thickness ($\frac{\pi r_0}{4} = 0.79 \text{ cm}$) corresponding to isotropic oblate ellipsoidal diffusion at the liquid disc, and one transient diffusion length ($\sqrt{\pi D t} = 1.8 \text{ cm}$ for the smallest time interval used, $t = 10 \text{ s}$, with typical vapour diffusion coefficients, D , given in Table 1 as *ca.* $0.1 \text{ cm}^2 \text{ s}^{-1}$). This design thus enables diffusion transport in the gas phase to occur in the directions normal and tangential to the liquid disc surface. The thick insulation also ensured that no back diffusion would take place, enabling a simplification of the system to well-known electrochemical theory at ultramicroelectrodes [18-20], whilst ensuring the time to reach the occurrence of steady-state concentration profiles in the gas phase would be minimised, thereby reducing experimental measurement time.

The filled cylindrical pot was placed on a calibrated analytical balance in a well-ventilated environment at ambient temperature ($21 \pm 2 \text{ }^\circ\text{C}$) and pressure (1 atm) with relative humidity of 50-70%. In order to keep the experimentation simple, the pot was not thermostatted in any way. In order to remove the influence of stray convective cross-flow from the ventilated environment, the pot was shielded by closing the doors of the balance. The mass of the pot filled with liquid was noted at 10, 30 or 60 s intervals using a timer, and recorded manually. Although the analytical balance used was calibrated annually, it is important to recognise that the manual logging of the data may incur systematic and

random errors. Evaporation rate (e) data were computed from these mass loss transients through simple numerical differentiation of the data in either Matlab or Microsoft Excel ($e = -\frac{dm}{dt} \approx -\frac{\Delta m}{\Delta t}$, using consecutive time and mass points), and then typically averaged over at least two experimental runs, so as to smooth out any outliers in the data.

3. Results and Discussion

We first consider experimental data pertaining to the evaporation study of pure solvents, before moving on to resin systems and, subsequently, manufactured inks.

3.1 Evaporation Studies on Pure Liquid Solvents

Figure 2 presents mass-time data recorded for five different solvents (toluene, IPAC, THF, MEK and water) from the PTFE pot described in §2.2, with the data normalised through the initial mass of the ink and pot at the start of the experiment (m_0). These plots clearly indicate the loss in mass due to solvent evaporation over time, for each solvent. However, it is clear that over the experimentation time, there is a non-constant mass loss: the mass loss plots are curved at the shortest of times, followed by a period of constant mass loss, and for the case of the most volatile solvents considered, THF and MEK, departure from constant mass loss occurs at much greater measurement times (typically after *ca.* 400 s).

Solvent evaporation from the liquid | air interface that is created by the “flat” circular “solvent disc”, of radius r_0 , can be considered as a diffusional process [23-29]. Although the experiments were not thermostatted, ignoring temperature effects, if the solvent contained in the PTFE chamber is an infinite supply that is well-mixed, and evaporates to yield a perfect gas, the interfacial boundary condition on the gas side is the saturation concentration (c_s) of the solvent vapour. Assuming the solvent to behave ideally, and that there is no evaporative cooling of the liquid surface that leads to a reduction of the vapour pressure [23-33], nor any surface heterogeneity present that gives rise to an increase in the vapour pressure as a result of the Kelvin equation [34] or through specific adsorption at the liquid | air interface, this is given by equation (1).

$$c_s = \frac{xp^*}{RT} \quad (1)$$

in which x is the mole fraction of the solvent in ideal solution ($x = 1$ for pure solvents), p^* is the vapour pressure of the pure solvent, R is the molar gas constant ($8.3145 \text{ J mol}^{-1} \text{ K}^{-1}$) and T is the absolute temperature. Since evaporation from the liquid disc surface to the semi-infinite gas phase is a diffusional process, if this is considered as occurring only through one-dimensional evaporation away from the disc surface, the *mass evaporation rate* (e), defined as the rate of mass gain into the gas phase, *viz.*

$$e = -\frac{dm}{dt} \quad (2)$$

in which m is the mass of the liquid remaining, can be considered to be the equivalent of the current flowing (the rate of change of interfacial charge transfer) in electrochemistry. Accordingly, it can be shown that evaporation rate can be given by an expression analogous to the Cottrell equation [35] in electrochemistry:

$$e = MS c_s \sqrt{\frac{D}{\pi t}} \quad (3)$$

where S is the geometric area of the exposed interface ($S = \pi r_0^2$), M is the molar mass of the evaporating species, and D is its vapour phase diffusion coefficient. Hence, by combining equations

(2) and (3), followed by integrating with the temporal boundary condition $t = 0$, $m = m_0$, the normalised mass loss decreases with the square root of the measurement time, equation (4):

$$1 - \frac{m}{m_0} = 2 \frac{M}{m_0} S c_s \sqrt{\frac{D t}{\pi}} \quad (4)$$

The plots illustrated in Figure 2, at least for measurement times less than 400 s reveal a marked deviation from that anticipated from equation (4). Accordingly, given the axisymmetric nature of the experimental set-up, we next consider the evaporative mass loss as occurring through cylindrical diffusion, in which diffusion in the gas phase may occur through anisotropic diffusion coefficients in the directions perpendicular to the surface (D_z) and tangential to the interface (D_r) [36-38]. This formulation enables the recognition of the potential for eddy diffusion in the direction normal to the interface (“vertical mixing”), owing to the solvent vapours all being heavier than air (1.2 kg m^{-3} , *q.v.* Table 1), thereby displacing air during the evaporation process, and inducing a concentration gradient of air at the liquid | gas interface, encouraging a buoyancy-driven convective flow [39,40]. Whilst the effect of natural convection is thought to provide a spatial dependence of the value of D_z [39-47], we assume D_z to be constant.

Thus, continuing with our electrochemical analogy, following the work by Aoki and Osteryoung [48], and Shoup and Szabo [49], the mass loss curves for two-dimensional mass loss in the gas phase are given by equations (5) and (6),

$$1 - \frac{m}{m_0} = 2 \frac{M}{m_0} S c_s \sqrt{D_z t} \left\{ \frac{1}{\sqrt{\pi}} + \frac{\sqrt{D_r t}}{2r_0} - \frac{3D_r t \sqrt{D_r t}}{2^8 r_0^3} + \dots \right\} \quad (5a)$$

$$1 - \frac{m}{m_0} = 4 \frac{M}{m_0} \sqrt{D_r D_z} r_0 c_s t \left\{ 1 + \frac{4r_0}{\sqrt{\pi^3 D_r t}} - \frac{8r_0^3}{\sqrt{(\pi D_r t)^3}} \left(\frac{1}{9} - \frac{1}{\pi^2} \right) + \dots \right\} \quad (5b)$$

$$1 - \frac{m}{m_0} = \frac{M}{m_0} r_0^3 c_s \sqrt{\frac{D_z}{D_r}} \left[\frac{\pi D_r t}{r_0^2} + \frac{2\sqrt{\pi D_r t}}{r_0} - 0.2627 \left\{ \frac{1}{2} \ln \left(\frac{0.3912 r_0}{\sqrt{D_r t}} \right) - \frac{0.1956 r_0}{\sqrt{D_r t}} + \frac{0.0191 r_0^2}{D_r t} - \frac{0.0017 r_0^3}{\sqrt{(D_r t)^3}} + \dots + \frac{1.2781 \sqrt{D_r t} \exp\left(\frac{0.3912 r_0}{\sqrt{D_r t}}\right)}{r_0} \left(1 - \frac{2.5563 \sqrt{D_r t}}{r_0} \right) \right\} \right] \quad (6)$$

As before, these equations have been derived through our “similarity principle” between evaporation rate and faradaic current, followed by integration. The formulation of equation (6) requires evaluation of an integral of the form $\int \frac{e^{-u}}{u^3} du$ which gives rise to the infinite series provided in the expression; the Appendix (§5) provides an overview of the derivation of these equations. Equations (5a) and (5b) correspond to the equivalent mass loss curves for short and long time, respectively, and stem from the Aoki-Osteryoung expressions for chronoamperometry at microdisc electrodes [50]; equation (6) originates from the Shoup-Szabo all-time expression for the same problem. Equations (5a) and (6) cover the case at small times ($t \rightarrow 0$) when axial diffusion dominates the transient, where it is seen that expression (5a) tends to that given by equation (4) where $D = D_z$; equations (5b) and (6) tend to a constant evaporation rate at long times ($t \rightarrow \infty$), for which the limiting evaporation rate, e_{lim} , is given by the expression,

$$e_{lim} = 4M\sqrt{D_r D_z} r_0 c_s \quad (7)$$

which is the evaporation equivalent to the steady-state current at a microdisc electrode, first derived by Saito for the case of isotropic diffusion ($D_r = D_z$) [51].

Based on the four organic solvents given in Table 1, the steady-state evaporation rate estimated by equation (7) ranges between 40 – 300 $\mu\text{g s}^{-1}$ at 293 K within our evaporation chamber of radius, $r_0 = 1.0$ cm, and indicates that *steady-state measurements may empower the development of a QA/QC testing procedure* as envisaged in §1. Accordingly, the experimental data in Figure 2 were compared with that predicted by equations (5) and (6), with the comparison depicted as the solid black lines in each plot in Figure 2, with the diffusion coefficients reported in Table 2. These calculations were made by assuming the gas phase tangential diffusion coefficient (D_r) takes the reported literature value of the vapour diffusion coefficient (*q.v.* Table 1), and, using the value of c_s inferred from equation (1) and the literature data reported in Table 1, the axial diffusion coefficient (D_z) was estimated from equations (5b)[‡] and (6), with the theoretical lines illustrated in Figure 2 being computed using equation (6). Clearly, there is excellent agreement between experiment and theory for all four solvents, at least with measurement times smaller than *ca.* 400 s – the coefficients of determination, R^2 , given by the expression [52],

$$R^2 = 1 - \frac{\text{Residual sum of squares}}{\text{Total sum of squares}} = \frac{\sum_i (y_i - \bar{y})^2}{\sum_i (y_i - \hat{y}_i)^2} \quad (8)$$

where y_i are the ordinate points corresponding to individual time points (x_i), \bar{y} is the arithmetic mean of the experimental points and \hat{y}_i are the individual points on the calculated regression line corresponding to the individual time points (x_i), are all greater than 0.8, and the relative standard deviations of the derived values of D_z range between 9-21%. Only in the cases of the most volatile solvents, THF and MEK, at long timescales (>400 s), is there a marked deviation between the experiment and theory. Furthermore, with the exception of the heaviest solvent (IPAC) which appears to give rise to isotropic transport in the gas phase, the solvents exhibit significant vertical mixing: D_z is larger than D_r by a factor ranging between approximately three and eight (*q.v.* Table 2).

The above analysis assumes that the axial diffusion coefficient is invariant with time, and therefore can be treated as a “true” average. Figure 3 shows the variation of the computed values of D_z with time. These are indeed invariant with time for the two heaviest solvents (IPAC and toluene), but both MEK and THF – solvents with identical molar masses, exhibit peaks in the trend of D_z with time. Moreover, in both cases, the reported error is largest at times smaller than *ca.* 400 s than it is above this time. Both THF and MEK have vapour pressures at 20 °C that are at least 10% of ambient, giving rise to faster mass loss than for IPAC and toluene. For these faster evaporating solvents, there are two points of inflection that occur at *ca.* 200 s and 400 s. Since 400 s corresponds to a one-dimensional diffusion layer thickness approximately equivalent to the depth of the liquid that is lost through evaporation

[‡]Note that since the smallest time interval is 10 s, for the specific dimensions of our system and typical literature vapour diffusion coefficients given in Table 1 of *ca.* 0.1 $\text{cm}^2 \text{s}^{-1}$, equation (5a) is not applicable, since it is valid only for $t \leq 3.6$ s, whilst equation (5b) is valid from $t \geq 2.05$ s. It thus follows that only equations (5b) and (6) need be used for comparison with experimental data.

during this time (*ca.* 0.1 cm), we suggest that this indicates that actually, D_r is not constant through the evaporation process, owing to the reducing level of the liquid in the cylinder – the system moves to the electrochemical equivalent of a “recessed” microdisc electrode during the course of experimentation. Thus, at longer measurement times, these liquids should start to move away from a steady-state regime, and tend to a one-dimensional transient case, so that the mass loss moves from being temporally invariant, to one that depends on the square root of the time (equations (4) and (5a)). This is indeed observed as demonstrated in Figure 4, where plots of $1 - \frac{m}{m_0}$ against $t^{1/2}$ exhibit curvature at all times for IPAC and toluene, but *linearity at longer times for MEK and THF*.

In contrasting the transport characteristics between MEK and THF, we suggest that the data may indicate a degree of association of the evaporated solvent species with atmospheric water, owing to the apparent paradox in the size of the apparent vapour diffusion coefficients for these solvents with identical molar masses. We next seek to translate these insights to the study of mixed solvent evaporation in the presence of other additives.

3.2 Evaporation Studies on Mixed Solvent Resins Systems

As illustrated in Figure 1, the resin, introduced during the let-down in the manufacture, is an important component of the final ink product, since it allows the dried pigments and filler particles to be fixed to the substrate during the printing process. Resins are produced by dissolving specific compounds (binders) into organic solvents [14-16]. Our inks tend to use mixed solvents, so as to afford a good drying of the ink for the particular method by which it is printed, and for the particular substrate on which it is to be printed. For example, the ink used to print Paris transportation tickets (FHL0201 – an ink that mainly uses IPAC as the solvent), needs to be suitable for the rotogravure press and substrate employed [53]; in contrast the ink used to print the London Underground and British Rail tickets (HL0301 – an ink comprising an MEK and IPAC mixture), needs to have faster evaporation rates at much lower temperatures, since thermally-sensitive, paper-based substrates are used. We consider the resins for these two different types of ink: for FHL0201, we have employed a resin (AR01) that mainly (*ca.* 99 mol%) comprises a mixture of two solvents, with other compounds making up the resin; for HL0301, we found that a mixture (HR01) of two solvents (*ca.* 80 mol%) with other binders works well.

Evaporative mass loss curves for these mixed-solvent resin systems are depicted in Figure 5. These plots are in the form $\frac{1 - \frac{m}{m_0}}{\sqrt{t}}$ vs. $t^{1/2}$ since steady-state vapour diffusion is considered to be the dominant transport pathway after $\vartheta = \frac{\pi r_0^2}{16D_z} = 0.3 - 2.6$ s, for the typical values of D_z given in Table 2 for the four organic solvents used. Thus ignoring measurements taken below 20 s, the shape of the observed plots is rationalised as follows. At short times, steady-state evaporation occurs – the evaporation rate is independent of time, causing the mass loss to be proportional to time. This gives rise to the straight line that is observed. At longer times, *depletion of the solvent from the resin system creates a diffusion barrier that curtails the evaporation rate*. Since diffusion in the liquid phase is typically 10^4 smaller

than diffusion in the gas phase, and recognising that diffusion in viscous polymer solutions is likely to be at least two orders of magnitude smaller than this (typical diffusion coefficients in polymers lie in the range $10^{-13} \leq D/\text{cm}^2 \text{ s}^{-1} \leq 10^{-5}$ [36-38]), the observed mass loss curve exhibits diffusion effects that are proportional to \sqrt{t} , in line with our expectation, and work reported by others [33]. Since we are unable to provide the exact composition of these commercially available materials, we do not provide a quantitative fit between experimental data and bespoke theory that looks at this transition.

As expected, resins comprising more volatile solvents (such as MEK and THF) afford higher rates of mass loss, as evidenced in Figure 5 through the comparison between the HR01 (more volatile solvents used, green diamonds) with the AR01 (a mixed solvent resin mainly containing IPAC, blue squares and red circles). The fact that the effects of diffusional depletion within the resin manifest later for HR01 than for AR01, likely reflects the faster diffusion of the lighter solvents in HR01 compared with AR01. Furthermore, the effects of poor experimentation are readily discernable through these mass loss curves: Figure 5 enables the comparison of evaporation measurements undertaken for the AR01 resin under closed (blue squares and red circles) *versus* open (magenta pentagons) conditions. In the latter, cross-ventilation was allowed to occur, to alter the boundary condition at the resin | gas interface. This results in higher evaporation rates, and the establishment of diffusion control through the resin sooner, as anticipated.

Thus, taken together, these results indicate that the evaporative mass loss curve is a sensitive marker for the nature of the solvent within the liquid phase. We next investigate evaporation rates from real, commercialised inks.

3.3 *Evaporation Studies from Commercialised Ink Products*

Our inks comprise suspended solid particles in a dispersion of organic binders, other polymers, other particles and mixed organic solvents. The inks are typically made by wet milling of pigment, with other additives, for several hours, followed by a let-down phase in which the resin is introduced and mixed into the formulation. Accordingly, the mole fractions of the individual solvents in the final ink are different to those present in the resin. Figure 6 depicts evaporative mass loss curves corresponding to two commercial ink products: HL0301 – low coercivity magnetic ink employed to create the magnetic stripe on British Rail tickets, and which comprises two solvents (MEK and THF) at *ca.* 80 mol%; and HH0501 – an high coercivity magnetic ink employed to manufacture tickets for Polish buses, which contains *three* solvents (MEK, THF and one other) at *ca.* 70 mol%. Both of these inks are manufactured for use through gravity-fed coating, and have specified Brookfield viscosities of 4000 ± 1000 cP (measured using a Brookfield viscometer fitted with a number 5 LVS spindle at 20 rpm for a minimum of 2 min, with a conversion factor of 200), and have different pigments – the low coercivity ink employs acicular γ -ferric oxide as the primary, ferrimagnetic pigment; the high coercivity ink uses a mixture of hexagonal alkaline-earth ferrites as the ferrimagnetic pigment.

The curves in Figure 6 exhibit similar features to those described in §3.2 – ignoring data at $t < 20$ s, at short times steady-state vapour diffusion away from the ink | gas interface controls the evaporation rate; this falls off at longer time owing to diffusion of the solvents to the interface within the ink phase. Since the solvent composition is different between the HL0301 ink and the HR01 resin that is used, the mass loss curves are different in Figures 5 and 6, and it is not possible to identify or extract any interfacial kinetic effects, or even the degree of self-inhibition of the surface stemming from the presence of solid particles at the interface thereby reducing the interfacial area, from the greater evaporation rate from the HL0301 ink compared with the HR01 resin. However, the larger solvent evaporation rate from HL0301 compared with HH0501 is consistent with the greater ratio of MEK:THF within these inks, in keeping with the vapour diffusion coefficients reported in Table 2.

It thus follows that, with the mixed solvents used, measurement timescales that probe *both* transport within the gas phase and in the ink, may provide a robust QA/QC tool; accordingly, we explore this in the next section.

3.4 Evaporation Rate Measurement as a QA/QC Tool

In May, 2018, a batch of HL0301 was manufactured which, caused a number of problem in its use, specifically an increased extent of “picking” of the printed goods during the windings. The “picking” of printed material results from incompletely dried ink interacting with, and subsequently adhering to, the *verso* side of the printed board as it is coiled-up for transfer of the printed roll to a different part of the factory floor for further processing. Both coating operators and those using the printed goods typically notice errors due to print “picking”, but at this point it is too late in the print manufacturing process and leads to expensive production downtime. Since the substrate used for the printing of HL0301 ink is sensitive to temperature, so that the ink dryers cannot be raised to higher temperatures, the batch of ink was suspected as being formulated using an incorrect solvent. Accordingly, testing, this ink gave the evaporation transients illustrated in Figure 6 (green diamonds in panel a; red circles in panel b). It is clear from the comparison with the standard HL0301 formulation (blue squares and red circles in panel a; blue squares in panel b) that the gas phase transport is similar for both standard and suspected ink, however, the transition to evaporation dominated by transport within the ink occurs sooner, and gives rise to smaller evaporation rates for the suspected ink compared with the standard formulation. Indeed, the gradient of the evaporation rate plot with $t^{-1/2}$ revealed that the suspected ink was found to be *ca.* 80% of that for the known standard HL0301 formulation (*q.v.* Figure 6b), indicating a less volatile solvent mixture had been used in its preparation. The identification of an incorrect formulation of this batch of ink is validated through the problems it caused when used during the printing of the ink in Hull in June, 2018; further investigation revealed an operator error, which would have otherwise not been able to be traced without incurring large testing expenses. It follows that evaporation rate measurement can serve as a valuable quality control tool for quality assurance during ink manufacturing processes, and its use can empower the early mitigation of human factor errors.

4. Conclusions

In this work, we have developed a simple and inexpensive approach to the QA/QC monitoring of the manufacture of printing inks, through the evaporative loss of the solvents used in its formulation. Inspired by electrochemical systems, we have developed theory that enables the theoretical evaporative rate transient to be readily calculated and compared with experimentally derived data. Experimental transients reveal that the evaporative loss is dominated by eddy diffusion in the vapour phase, and the extent of this is related to the nature of the evaporating solvent, so that incorrect ink formulations can be readily identified. This is important because, as a quality control tool for quality assurance, it can prevent manufactured goods from not conforming to customer expectation and specification. We note that this approach can be exploited for permeation measurements through thick polymer membranes [54]. Furthermore, although the gravimetric measurements undertaken in this work comprise a “rough and rugged” approach, the design of the evaporation chamber used empowers a simplicity in the operational deployment of this “tool”: this type of measurement is advantageous compared with the conventional Stefan-Winklemann approach since there is no need to flow gas at some distance away so as to impose a Neumann boundary condition, since this is naturally imposed at semi-infinite distances from the liquid | gas interface. This then reduces the cost of the experimental equipment needed, and the procedures and protocols for the measurement are at a level sufficiently appropriate for operators to undertake with minimum training, thereby encouraging an increase in productivity and GVA.

Acknowledgements

We thank BemroseBooth Paragon, Ltd. together with InnovateUK and the Engineering and Physical Sciences Research Council for funding this work through two Knowledge Transfer Partnerships (Programme Numbers 9576 and 10844). HJW and TAA-T both thank The University of Hull for funding their postgraduate research studies. We thank Jordan Elliott, Erika M. Brito, Leonardo A. de Oliveira Roque, Paula A. Silva, Tony R. A. de Souza, João V. L. Umbelino, Adriana P. Kern, Carolina B. O. Silva and Sandro A. Steinhorst for undertaking preliminary experiments, during their undergraduate projects at The University of Hull between 2014-2016. It is a pleasure to acknowledge Howard Snelling and Neil Kemp (both University of Hull), Dominique Durant des Aulnois (ParagonID, S.A.), Rob Burgin (BemroseBooth Paragon), Andrew Jones (ParagonID), Paul McEnaney (Paragon Europe) and François Gauthier (Paragon Identification S.A.S.) for helpful discussions and for their support for this work. We are grateful to one of the anonymous reviewers for encouraging us to develop equations (5) and (6).

Dedication

This paper is dedicated to Professor Richard G. Compton (Oxford University, UK) in honour of his 65th birthday.

5. Appendix: Derivation of Equations (5) and (6)

Following Saito [51], for the axisymmetric, cylindrical case considered in which only diffusive mass transport in the gas phase is significant, Fick's second law gives the time-dependent evaporation flux:

$$\frac{\partial c}{\partial t} = D \left\{ \frac{\partial^2 c}{\partial r^2} + \frac{1}{r} \frac{\partial c}{\partial r} + \frac{\partial^2 c}{\partial z^2} \right\} \quad (\text{A1})$$

where the c is the concentration of the vapour, r is the co-ordinate tangential to the liquid disc surface, z is the co-ordinate normal to the disc surface, and D is the vapour diffusion coefficient of the evaporating solvent. Defining the point of $z = 0$ as the liquid | gas interface, for the gas phase, initially free from the evaporating solvent, and with rapid vaporisation being established at the liquid | gas interface, the relevant boundary conditions for the solution of equation (A1) are as follows, with c_s representing the surface concentration of the pure liquid vapour.

Initial conditions:

$$t \leq 0 \quad c = 0 \quad \forall r, z$$

Time-dependent conditions:

$$\text{Interface:} \quad t > 0 \quad c = c_s \quad r \leq r_0, z = 0$$

$$\text{Insulation boundary:} \quad \frac{\partial c}{\partial z} = 0 \quad r > r_0, z = 0$$

$$\text{Symmetry axis:} \quad \frac{\partial c}{\partial r} = 0 \quad r = 0, \forall z$$

$$\text{Semi-infinite boundary:} \quad c \rightarrow 0 \quad r, z \rightarrow \infty$$

Comparison of these boundary conditions to those formulated by Saito [51] for steady-state diffusion to a microdisc electrode, and defining the evaporation rate, e , as:

$$e = -\frac{dm}{dt} = M \int j dS \quad (\text{A2})$$

suggests the steady-state evaporation rate, e_{lim} , is given by:

$$e_{lim} = 4MDr_0c_s \quad (\text{A3})$$

and resembles the classical expression for the limiting current at a microelectrode. This gives the ‘‘similarity principle’’ between equations for evaporation rate and electrochemical systems that ‘‘current is equivalent to evaporation rate’’, ‘‘the weighted stoichiometric molar charge is equivalent to the molar mass of the evaporating solvent’’, and ‘‘the bulk concentration of the analyte is equivalent to the saturation concentration of the evaporating solvent.’’ Using this similarity principle, equation (3) in the main text can be readily discerned from the Cottrell equation.

In order to deal with the case where anisotropic diffusion in the vapour arises, owing to the occurrence of natural convection induced ‘‘vertical mixing’’ above the liquid disc, we employ our previous ‘‘law’’ that analytical expressions for axisymmetric anisotropic diffusion are identical to those for isotropic diffusion, provided the geometric mean of the direction-dependent diffusion coefficients is used as the ‘‘average’’ value, with the dimensionless time being given exclusively in terms of the radial diffusion coefficient [36-38].

We next illustrate the derivations of the time-dependent mass loss expressions given by equations (5) and (6) in the main text. For the case of chronoamperometry at microdisc electrodes, and noting that the dimensionless time, τ , is:

$$\tau = \frac{4Dt}{r_0^2} \quad (\text{A4})$$

Aoki and Osteryoung [48] developed the following expressions for the time dependence of the dimensionless current, ψ , reported by Wightman and Wipf [50].

$$\psi = \frac{1}{2} \sqrt{\frac{\pi}{\tau}} + \frac{\pi}{4} - \frac{3\pi}{2^{10}} \tau + \dots \quad \tau \leq 1.44 \quad (\text{A5a})$$

$$\psi = 1 + \frac{4}{\sqrt{\pi^3 \tau}} + \frac{32}{\sqrt{\pi^3 \tau^3}} \left(\frac{1}{9} - \frac{1}{\pi^2} \right) + \dots \quad \tau \geq 0.82 \quad (\text{A5b})$$

These are the short- and long-time expressions, which overlap in the range $0.82 \leq \tau \leq 1.44$. As noted by Wightman and Wipf [50] they are “rather cumbersome for routine use with experimental data.” Accordingly, the all-time expression determined by Shoup and Szabo [49], which is accurate to 0.6% for all times, is often preferred for treating experimental data:

$$\psi = 0.7854 + \frac{1}{2} \sqrt{\frac{\pi}{\tau}} + 0.2146 \exp\left(-\frac{0.7824}{\sqrt{\tau}}\right) \quad (\text{A6})$$

The transformation of equations (A5) and (A6) into equations (5) and (6) in the main text, relies on the use of the similarity principles discussed above, noting that the dimensionless evaporation rate is given as:

$$\psi = \frac{e}{4M\sqrt{D_r D_z} r_0 c_s} \quad (\text{A7})$$

and, given equation (2) in the main text defines the evaporation rate (e), integration of equation (A7) under the boundary condition $\tau = 0$, $m = m_0$, yields the time-dependent mass-loss curves.

$$1 - \frac{m}{m_0} = \frac{M}{m_0} r_0^3 c_s \sqrt{\frac{D_z}{D_r}} \int \psi d\tau \quad (\text{A8})$$

The expressions in equation (A5) are readily straightforward to integrate, and afford, ignoring integration constants:

$$\int \psi d\tau = \sqrt{\pi\tau} + \frac{\pi}{4} \tau - \frac{3\pi}{2^{11}} \tau^2 + \dots \quad \tau \leq 1.44 \quad (\text{A9a})$$

$$\int \psi d\tau = \tau + 8 \sqrt{\frac{\tau}{\pi^3}} - \frac{64}{\sqrt{\pi^3 \tau}} \left(\frac{1}{9} - \frac{1}{\pi^2} \right) + \dots \quad \tau \geq 0.82 \quad (\text{A9b})$$

Thus, the combination of equations (A4), (A8) and (A9) yields the expressions given in equation (5) of the main text.

The derivation of equation (6) from equation (A6) requires the substitution $u^2 = \frac{0.6121}{\tau}$ thereby enabling the deduction that,

$$\int \psi d\tau = 0.7854\tau + \sqrt{\pi\tau} - 0.2627 \left\{ \frac{1}{2} \ln(u) - \frac{u}{2} + \frac{u^2}{8} - \frac{u^3}{36} + \dots + \frac{e^{-u}(u-1)}{2u^2} \right\} \quad (\text{A10})$$

where integration constants have again been ignored. The infinite series in equation (A10) stems from the result $\int \frac{e^{-u}}{u} du = \ln(u) - u + \frac{u^2}{2(2!)} - \frac{u^3}{3(3!)} + \dots$. Thus, the combination of equations (A4), (A8) and (A10) gives rise to equation (6) in the main text.

References

1. See, for example, S. Rawlinson, A. McLister, P. Kanyong, J. Davis, Rapid determination of salicylic acid at screen-printed electrodes, *Microchem. J.*, 2017, **137**, 71.
2. C. C. Dai, P. Song, J. D. Wadhawan, A. C. Fisher, N. S. Lawrence, Screen-printed alizarin-based carbon electrodes: monitoring pH in unbuffered media, *Electroanalysis*, 2015, **27**, 917.
3. <https://pubchem.ncbi.nlm.nih.gov/compound/Tetrahydrofuran> (accessed on January 15, 2020).
4. https://www.shell.com/business-customers/chemicals/our-products/solvents-chemical/ketones/_jcr_content/par/tabbedcontent/tab/textimage.stream/1459943761987/aa4a0ecc902a57b7ba182491ba379c14133dfab1/mek-s1213-global.pdf (accessed on January 15, 2020).
5. <https://pubchem.ncbi.nlm.nih.gov/compound/Isopropyl-acetate> (accessed on January 15, 2020).
6. <https://pubchem.ncbi.nlm.nih.gov/compound/Toluene> (accessed on January 15, 2020).
7. <http://www.inchem.org/documents/icsc/icsc/eics0179.htm> (accessed on January 15, 2020).
8. <https://www.gsi-net.com/en/publications/gsi-chemical-database/single/506-CAS-109999.html> (accessed on January 15, 2020).
9. G. A. Lugg, Diffusion coefficients of some organic and other vapours in air, *Anal. Chem.*, 1968, **40**, 1072.
10. C. R. Wilke, C. Y. Lee, Estimation of diffusion coefficients for gases and vapours, *Ind. Eng. Chem.*, 1955, **47**, 1253.
11. <https://www.gsi-net.com/en/publications/gsi-chemical-database/single/354-CAS-78933.html> (accessed on January 15, 2020).
12. J. Benítez, *Principles and Modern Applications of Mass Transfer Operations*, 2nd edn., Wiley, Hoboken, 2009.
13. D. R. Lide (ed.), *CRC Handbook for Chemistry and Physics*, 74th edn., CRC Press, Boca Raton, 1995.
14. H. Mollet, A. Grubenmann, *Formulation Technology: Emulsions, Suspensions, Solid Foams*, Wiley-VCH, Weinheim, Germany, 2001.
15. E. Papirer, E. Walter, A. Vidal, B. Siffert, H. Jakusch, Preparation of magnetic inks: adsorption of macromolecular dispersion agents on magnetic metallic iron pigments and electrical charge formation, *J. Colloid Interfac. Sci.*, 1997, **193**, 291.
16. K. O'Grady, R. G. Gilson, P. C. Hobby, Magnetic pigment dispersions: a tutorial review, *J. Magnet. Mag. Mater.*, 1991, **95**, 341.
17. H. J. Ward, Design development and construction of an ATEX-compliant ISO 9001:2008 magnetic ink manufacturing facility, *M. Sc. Thesis*, The University of Hull, 2018.
18. See, for example, P. J. Welford, J. Freeman, S. J. Wilkins, J. D. Wadhawan, C. E. W. Hahn, R. G. Compton, Laminated microelectrodes: a simple approach to the construction of inexpensive microelectrodes with a variety of geometries, *Anal. Chem.*, 2001, **73**, 6088.
19. L. J. Li, M. Fleischmann, L. M. Peter, Microelectrode studies of lead acid battery electrochemistry, *Electrochim. Acta*, 1989, **34**, 459.
20. C. Amatore, Ultramicroelectrodes: their basic properties and their use in semi-artificial synapses, *C. R. Acad. Sci. Ser. II B*, 1996, **323**, 757.
21. See, for example, R. E. Treybal, *Mass Transfer Operations*, 2nd edn., McGraw-Hill, New York, 1968.
22. R. Chhabra, V. Shankar, *Coulson and Richardson's Chemical Engineering: Volume 1B: Heat and Mass Transfer: Fundamentals and Applications*, 7th edn., Butterworth-Heinemann, Oxford, 2018.
23. K. J. Beverley, J. H. Clint, P. D. I. Fletcher, Evaporation rates of pure liquids measured using a gravimetric technique, *Phys. Chem. Chem. Phys.*, 1999, **1**, 149.
24. K. J. Beverley, J. H. Clint, P. D. I. Fletcher, S. Thubron, Evaporation rates of water contained within porous silica particles, *ibid.*, 1999, **1**, 909.
25. J. H. Clint, P. D. I. Fletcher, I. T. Todorov, Evaporation rates of water from water-in-oil microemulsions, *ibid.*, 1999, **1**, 5005.
26. K. J. Beverley, J. H. Clint, P. D. I. Fletcher, Evaporation rates of structured and non-structured liquid mixtures, *ibid.*, 2000, **2**, 4173.
27. I. Aranberri, B. P. Binks, J. H. Clint, P. D. I. Fletcher, Evaporation rates of water from concentrated oil-in-water emulsions, *Langmuir*, 2004, **20**, 2069.
28. B. P. Binks, P. D. I. Fletcher, B. L. Holt, P. Beaussoubre, K. Wong, Selective retardation of perfume oil evaporation from oil-in-water emulsions stabilised by either surfactant or nanoparticles, *ibid.*, 2010, **26**, 18024.
29. B. P. Binks, P. D. I. Fletcher, A. J. Johnson, I. Marinopoulos, J. M. Crowther, M. A. Thompson, Evaporation of particle-stabilised emulsion sunscreen films, *ACS Appl. Mater. Interfaces*, 2016, **8**, 33.
30. Y. V. Borodacheva, V. A. Lotkhov, V. V. Dil'man, N. N. Kulov, Kinetics of the steady-state evaporation of single-component liquids into an inert gas, *Theoret. Found. Chem. Eng.*, 2011, **45**, 805.
31. V. A. Vlasov, Modelling of evaporation and condensation processes: a chemical kinetics approach, *Heat Mass Transf.*, 2018, **55**, 1661.
32. A. Kabalnov, H. Wennerström, Diffusion in evaporating solutions, *Soft Matter*, 2009, **5**, 4712.
33. K. Roger, E. Sparr, H. Wennerström, Evaporation, diffusion and self-assembly at drying interfaces, *Phys. Chem. Chem. Phys.*, 2018, **20**, 10430.
34. See, for example, R. J. Hunter, *Introduction to Modern Colloid Science*, Oxford University Press, Oxford, 1993.
35. Southampton Electrochemistry Group, *Instrumental Methods in Electrochemistry*, Horwood Publishing, Chichester, 2001.
36. L. A. Evans, M. J. Thomasson, S. M. Kelly, J. Wadhawan, Electrochemical determination of diffusion anisotropy in molecularly structured materials, *J. Phys. Chem. C*, 2009, **113**, 8901.
37. J. E. Halls, N. S. Lawrence, J. D. Wadhawan, Electrochemical estimation of diffusion anisotropy of N,N,N',N'-tetramethyl-*para*-phenylenediamine within the normal hexagonal lyotropic mesophase of Triton X 100/light water: when can the effects of cross-pseudophase electron transfer be neglected for partitioned reagents? *J. Phys. Chem. B*, 2011, **115**, 6509.
38. J. E. Halls, R. W. Bourne, K. J. Wright, L. I. Partington, G. M. Tamba, Y. Zhou, T. Ramakrishnappa, G. H. Mehl, S. M. Kelly, J. D. Wadhawan, Electrochemistry of organometallic lyotropic chromonic liquid crystals, *Electrochem. Commun.*, 2012, **19**, 50.
39. See, for example, R. P. Wayne, *Chemistry of Atmospheres*, 2nd edn., Oxford University Press, Oxford, 1991.
40. A. A. Kalinske, C. L. Pien, Eddy Diffusion, *Ind. Eng. Chem.*, 1944, **36**, 220.
41. B. Levich, The theory of concentration polarisation, *Discuss. Faraday Soc.*, 1947, **1**, 37.

42. J. S. Newman, *Electrochemical Systems*, Prentice-Hall, Englewood Cliffs, 1973.
43. C. Amatore, S. Szunerits, L. Thouin, J.-S. Warkocz, The real meaning of Nernst's steady diffusion layer concept under non-forced hydrodynamic conditions: a simple model based on Levich's seminal view of convection, *J. Electroanal. Chem.*, 2001, **500**, 62.
44. K. Ngamchuea, S. Eloul, K. Tschulik, R. G. Compton, Advancing from rules of thumb: quantifying the effects of small density changes in mass transport to electrodes: understanding natural convection, *Anal. Chem.*, 2015, **87**, 7226.
45. X. Li, C. Batchelor-McAuley, J. K. Novev, R. G. Compton, A thermostatted cell for electrochemistry: minimising natural convection and investigating the role of evaporation and radiation, *Phys. Chem. Chem. Phys.*, 2018, **20**, 11794.
46. J. K. Novev, R. G. Compton, Natural convection effects in electrochemical systems, *Curr. Opin. Electrochem.*, 2018, **7**, 118.
47. B. Dollet, F. Boulogne, Natural convection above circular discs of evaporating liquids, *Phys. Rev. Fluids*, 2017, **2**, 053501.
48. K. Aoki, J. G. Osteryoung, Formulation of the diffusion-controlled current at very small stationary disc electrodes, *J. Electroanal. Chem.*, 1984, **160**, 355.
49. D. Shoup, A. Szabo, Chronoamperometric current at finite disc electrodes, *J. Electroanal. Chem.*, 1982, **140**, 237.
50. R. M. Wightman, D. O. Wipf, Voltammetry at ultramicroelectrodes, in A. J. Bard (ed.), *Electroanalytical Chemistry*, volume 15, Marcel Dekker, New York, 1989, p.267.
51. Y. Saito, A theoretical study on the diffusion current at the stationary electrodes of circular and narrow band types, *Rev. Polarog.*, 1968, **15**, 177.
52. J. N. Miller, J. C. Miller, *Statistics and Chemometrics for Analytical Chemistry*, 5th edn., Pearson, Prentice Hall, London, 2005.
53. G. Thonnat, *Petite histoire du ticket de métro parisien*, éditions TELEMAQUE, Paris, 2010.
54. J. D. Wadhawan, B. Craster, N. S. Lawrence, S. M. Kelly, Regular solution theory for polymer permeation transients: a toolkit for understanding experimental waveshapes, *Langmuir*, in press; DOI: 10.1021/acs.langmuir.0c00589.

Table 1: Physical properties of the four solvents used in this work at 20 °C.

Property	THF	MEK	IPAC	Toluene
Molar Mass /kg kmol ⁻¹	72.11	72.11	102.13	92.14
Liquid Density /kg m ⁻³	883.3 ^a	805 ^b	874 ^c	862.3 ^d
Vapour Density Relative to Air	2.5 ^a	2.41 ^e	3.52 ^c	3.14 ^d
Vapour	9.36 ^f	9.03 ^g	7.70 ^g	8.49 ^g
Diffusion		8.92 ^h	7.53 ^h	7.83 ^h
Coefficient /10 ⁻² cm ² s ⁻¹		8.08 ⁱ		8.49 ^j
	Mean^k = 9.36	Mean^k = 8.55	Mean^k = 7.70	Mean^k = 8.49
Vapour Pressure at 20 °C and 1.0 atm /kPa	21.2 ^f	10.5 ^e	5.60 ^c	2.80 ^d
	19.3 ^a	9.50 ^b		3.79 ^l
	21.6 ^l	12.6 ^l		
	Mean^k = 20.3	Mean^k = 10.9	Mean^k = 5.60	Mean^k = 3.29

^aReference 3.

^bReference 4.

^cReference 5.

^dReference 6.

^eReference 7.

^fReference 8 (experimental value).

^gReference 9 (experimental value at 25 °C).

^hReference 9 (value estimated using the Wilke-Lee method¹⁰ at 25 °C).

ⁱReference 11 (experimental value).

^jReference 12 (experimental value at 25 °C).

^kArithmetic mean from experimentally given values, using both data at 20 °C and 25 °C.

^lReference 13.

Table 2: Extracted Diffusion Coefficients for Pure Solvents

Solvent	Literature Data $10^2 D /$ $\text{cm}^2 \text{s}^{-1}$	Literature Vapour Pressure/kPa	$10^2 D_r$ $/\text{cm}^2 \text{s}^{-1}$	$10^2 D_z^\dagger$ $/\text{cm}^2 \text{s}^{-1}$	D_z/D_r
THF	9.36	20.3	9.36	25.2 ± 4.4	2.70
MEK	8.55	10.9	8.55	70.4 ± 14.8	8.24
IPAC	7.70	5.60	7.70	7.34 ± 1.13	0.95
Toluene	8.49	3.29	8.49	26.9 ± 2.5	3.17

[†]Estimated as the mean over the full transient of the value of D_z estimated using equations (5b) and (6), averaged over the number of transients available (*q.v.* Figure 2), with the error representing one standard deviation from the full data set.

Figure Legends

Figure 1

Process flow diagram for ink manufacture.

Figure 2

Experimental mass loss curves, normalised by the initial mass, for the four pure solvents investigated: (a) THF (blue squares, $n = 2$), (b) MEK (red circles, $n = 3$), (c) IPAC (green diamonds, $n = 2$), and (d) toluene (magenta pentagons, $n = 2$). In each case, the error bars represent one standard deviation over the sample size (n). The black curve is that theoretically calculated using equation (6) and the anisotropic diffusion coefficients reported in Table 2, with coefficients of determination, R^2 of (a) 0.9754, (b) 0.8142, (c) 0.9999, and (d) 0.9989.

Figure 3

Variation of the estimated axial diffusion coefficient with time for the four organic solvents listed in Table 1. Key as for Figure 2.

Figure 4

Mass loss curves from Figure 2 re-plotted to illustrate the linear dependence at long time for THF and MEK solvents. Key as for Figure 2.

Figure 5

Comparison of experimental evaporative mass loss transients for two resins manufactured for two commercial products: AR01 (blue squares and red circles correspond to measurements from different batches manufactured in April, 2018, with the error bars representing one standard deviation for $n = 2$ in both cases, with measurements undertaken under closed conditions – see text; magenta pentagons represent measurements from a batch manufactured in January 2016, $n = 1$, with measurements undertaken under open conditions – see text); and HR01 (green diamonds, $n = 1$, with measurements undertaken under closed conditions) from a batch manufactured in December, 2015.

Figure 6

Evaporation mass loss transients corresponding to manufactured inks, with measurements undertaken under closed conditions: (a) HL0301 (transients from two batches manufactured between May - June, 2018 are illustrated as blue squares, $n = 2$, and red circles, $n = 2$, and a batch manufactured in May, 2018 suspected of being formulated with an incorrect solvent depicted as green diamonds, $n = 2$) and HH0501 (magenta pentagons, $n = 1$) manufactured in October, 2015; (b) comparison of evaporation rate transients between correctly manufactured HL0301 magnetic ink (blue squares, $n = 2$) and the suspected formulation (red circles). The error bars represent one standard deviation. In (b), the plot has been selected to emphasise the occurrence of limitations due to one-dimensional transport through the ink.

Figure 1

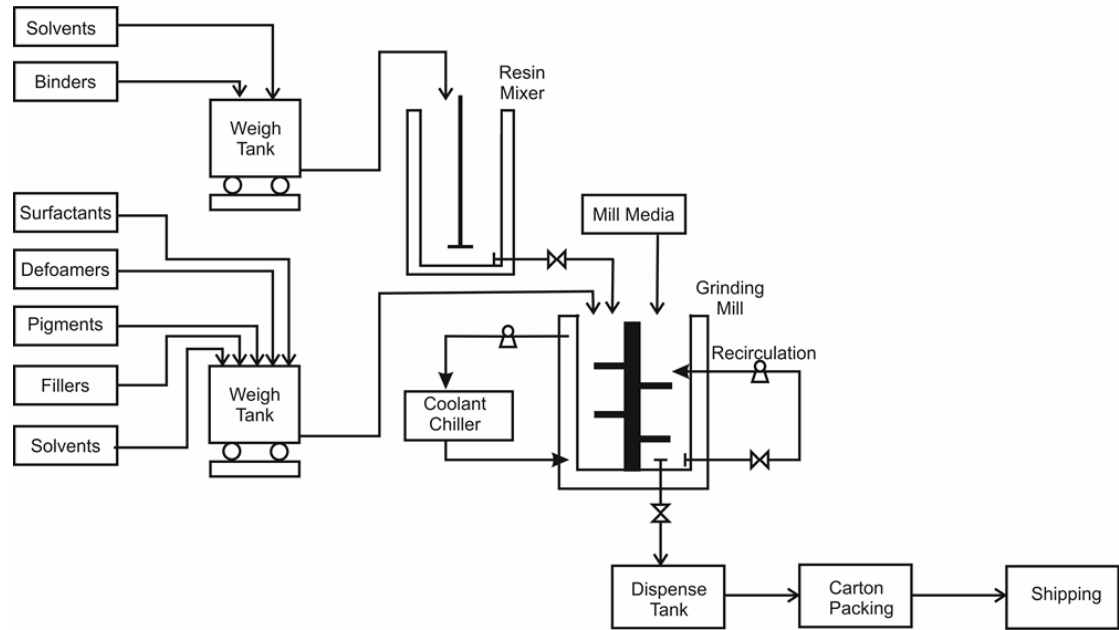
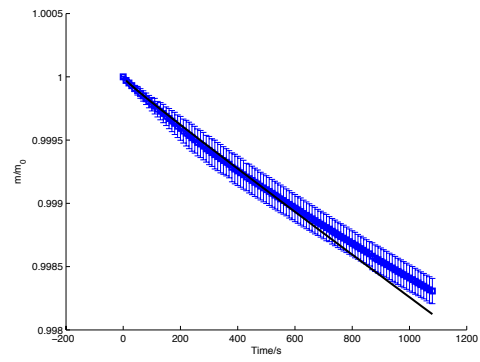
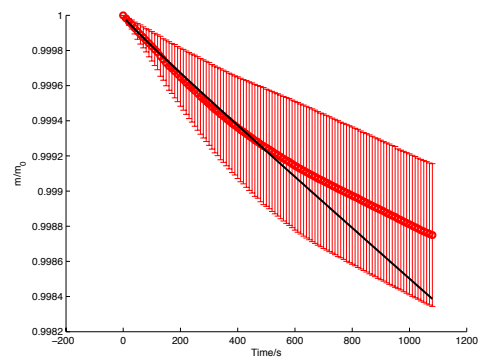


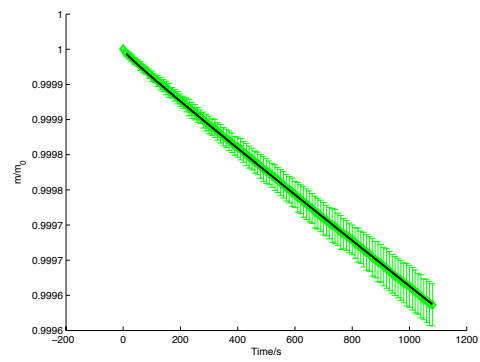
Figure 2
(a)



(b)



(c)



(d)

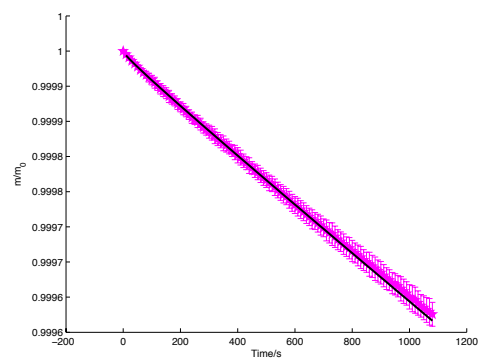


Figure 3

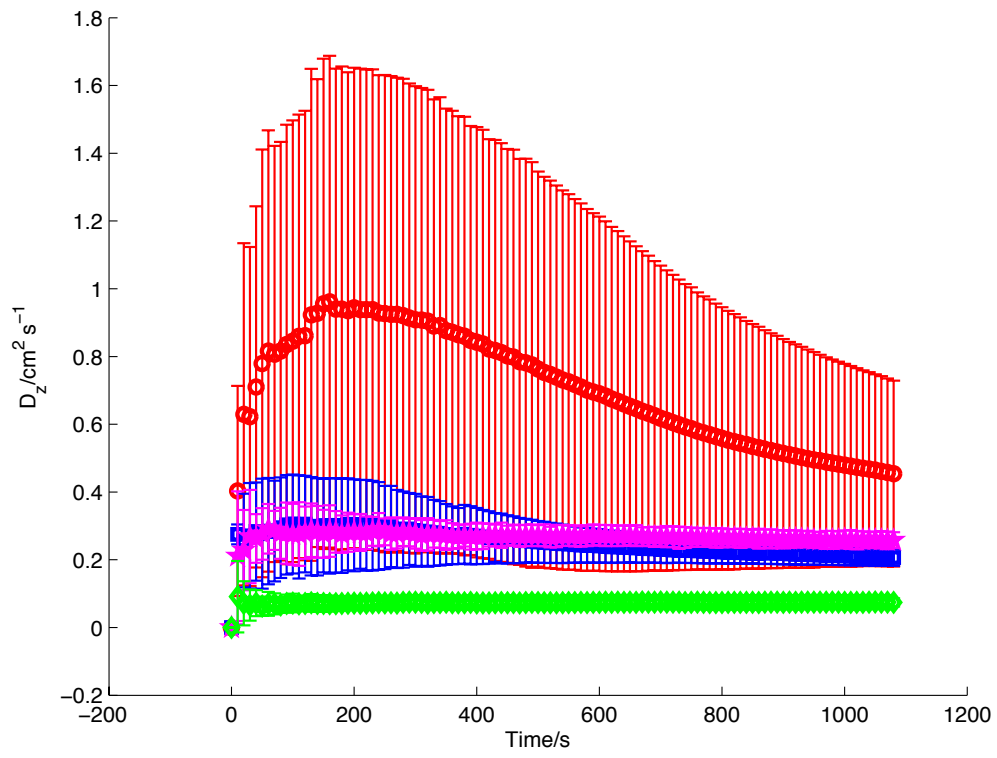


Figure 4

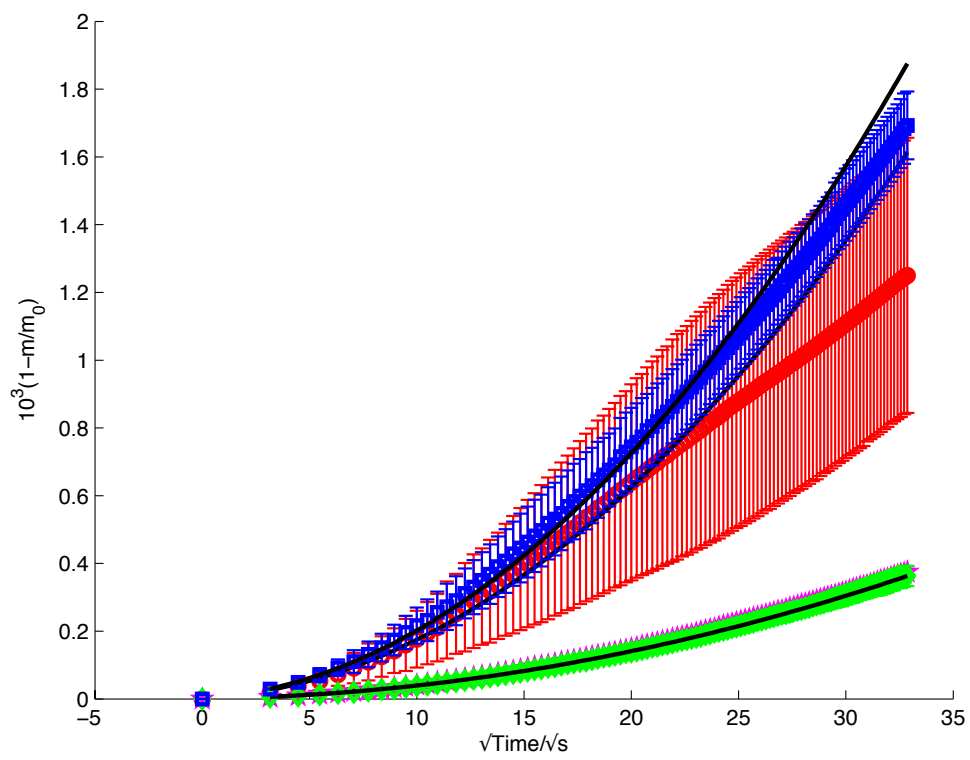


Figure 5

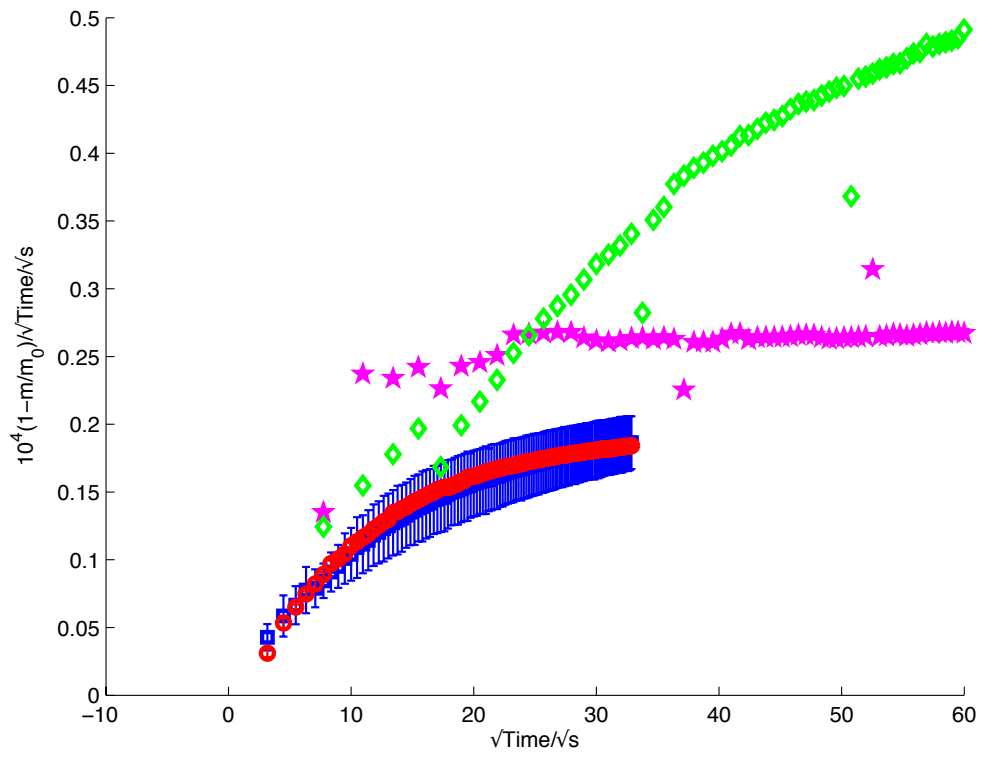
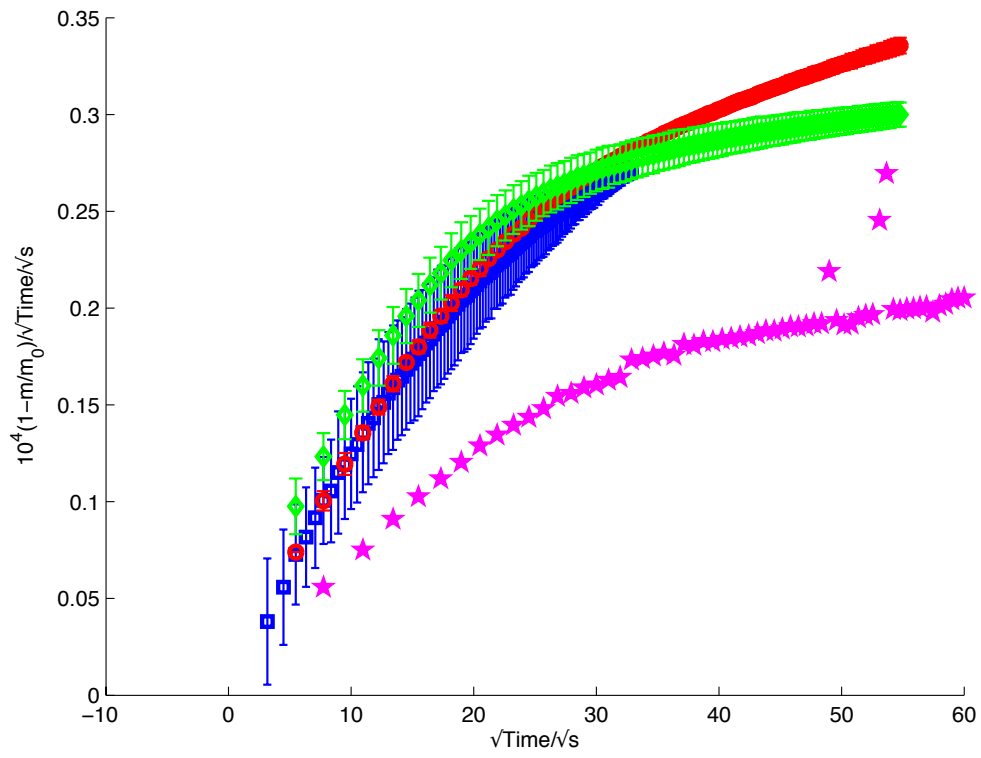


Figure 6
(a)



(b)

